Analytical Plasma Modelling and Design Upgrade for an ECR Thruster Operating on Water and Ammonia Propellants

IEPC-2019-638

Presented at the 36th International Electric Propulsion Conference
University of Vienna, Austria
September 15-20, 2019

E. Rosati Azevedo[1], D. Staab[2], A. Frey[3], L. Shadbolt[4] and A. Garbayo[5]
AVS UK Ltd., Rutherford Appleton Laboratory, Oxfordshire, OX11 0QX, United Kingdom

B. Karadag[6], R. Moloney[7], S. Masillo[8] and A. Lucca Fabris[9]
Surrey Space Centre, University of Surrey, Guildford, GU2 7XH, United Kingdom

and

O. Tarvainen[10], D. Faircloth[11], and S. Lawrie[12]
STFC ISIS, Rutherford Appleton Laboratory, Oxfordshire, OX11 0QX, United Kingdom

Abstract: Electrodeless plasma thrusters, and in particular Electron Cyclotron Resonance (ECR) thrusters, are attracting an increasing amount of commercial and academic interest by virtue of their ability to function without a neutralizer. This opens the door to operation with a wide range of alternative propellants all the while ensuring mitigation of some of the major life limiting erosion issues plaguing established technologies like Gridded Ion Engines and Hall Effect Thrusters. Building on the success of the proof-of-concept ECR thruster AQUAJET, the AQUAJET|NJET|XJET consortium, comprised of AVS UK Ltd., the University of Surrey, STFC ISIS, Viper RF, and Surrey Satellite Technology Ltd., have undertaken a follow on project to design, build, and test an improved thruster model capable of operating on water, xenon, and ammonia propellants. In the context of this project, analytical plasma modelling of water and ammonia discharges was undertaken. In the case of water discharge, these analyses revealed that at low electron temperatures (less than 6 eV) a significant fraction of energy is being dissipated to molecular dissociation. These analyses also allowed us to conclude that ammonia discharge can be expected to be slightly better than water in terms of power efficiency. Feasibility of ammonia operation was thus confirmed. We also describe the design upgrade of the AQUAJET breadboard, namely the improvements made to its microwave line, and to several of its key components.

[1]Electric Propulsion Engineer, AVS UK, erosati@a-v-s.uk
[2]R&D Engineer, AVS UK, dstaab@a-v-s.uk.com
[3]Space Project Manager, AVS UK, afrey@a-v-s.uk.com
[4]Project Engineer, AVS UK, lshadbolt@a-v-s.uk.com
[5]Business Development Director, AVS UK, agarbayo@a-v-s.uk.com
[6]Research Fellow, Surrey Space Center, b.karadag@surrey.ac.uk
[7]Ph.D. Candidate, Surrey Space Center, r.moloney@surrey.ac.uk
[8]Ph.D. Candidate, Surrey Space Center, s.masillo@surrey.ac.uk
[9]Lecturer in Space Propulsion/Electric Propulsion, Surrey Space Center, a.luccafabris@surrey.ac.uk
[10]Rutherford International Fellow, STFC ISIS, olli.tarvainen@stfc.ac.uk
[11]Low Energy Beams Group Leader, STFC ISIS, dan.faircloth@stfc.ac.uk
[12]Ion Source Section Leader, STFC ISIS, scott.lawrie@stfc.ac.uk

Nomenclature

DEA	= Dissociative Electron Attachment
E	= Average Energy Dissipated in a Collision, eV
ECR	= Electron Cyclotron Resonance
EP	= Electric Propulsion
$EVDF$	= Electron Velocity Distribution Function
GIE	= Gridded Ion Engine
HET	= Hall Effect Thruster
I_{SP}	= Specific Impulse
k	= Boltzmann Constant, $J.K^{-1}$
L	= Characteristic Plasma Dimension, m
m_e	= Mass of an Electron, kg
m_i	= Mass of an Ion, kg
n_-	= Number Density of Negative Ions, $particles.m{-}3$
n_+	= Number Density of Positive Ions, $particles.m{-}3$
n_e	= Number Density of Electrons, $particles.m{-}3$
n_n	= Number Density of Neutral Particles, $particles.m{-}3$
$NSTP$	= National Space Technology Programme
P_{beam}	= Beam Power, W
P_{in}	= Input Power, W
Q/M	= Charge to Mass Ratio, $C.kg^{-1}$
$STFC$	= Science and Technology Facilities Council
T_e	= Electron Temperature, eV
v	= Velocity, $m.s^{-1}$
v_B	= Bohm Velocity, $m.s^{-1}$
v_e	= Electron Velocity, $m.s^{-1}$
v_i	= Ion Velocity, $m.s^{-1}$
$\|\Delta\Phi_{sh}\|$	= Sheath Potential
η	= Electronegativity
η_D	= Beam Coupling Efficiency
η_{MW}	= Microwave Efficiency
η_T	= Thrust Efficiency
σ	= Cross Section, m^2
τ	= Confinement Time, s
χ	= Fractional Cost of the Energy Loss
ψ_{ion}	= Ionization Cost, $eV.ion^{-1}$

I. Introduction

Heritage technologies like GIEs and HETs have time and again proven to be quite successful, featuring not only on legacy missions like Deep Space 1, SMART-1, and Dawn,[1,2] but also featuring at the core of recent satellite propulsion design. SpaceX's Starlink constellation as a case in point.[3] Electrodeless plasma thrusters are nevertheless attracting an increasing amount of interest as next generation propulsion systems. The quasineutral exhaust plume generated by the ambipolar plasma expansion in these thrusters removes the need for an external neutralizing cathode to maintain spacecraft charge neutrality. As neutralizers are fragile systems, getting rid of this component can lead to longer thruster lifetime, higher reliability, and lower system cost.[4] Neutralizers are moreover highly sensitive to impurities. Eliminating this component therefore also eliminates reliance on high purity, pricey noble gases like Xenon. This opens the door to a wide range of cost effective alternative propellants, including molecular gases like CO_2, O_2, and H_2O.[5] Water has the added benefit of not requiring highly pressurized storage, making it particularly well suited for ride-share launches. Currently available water operated small sat thrusters relying on electrothermal and electrolysis technologies[6,7] are limited to I_{SP} values on order of 180 to 310 seconds. In theory, an appreciably higher ISP, over 1000 seconds, can be attained with an ECR device operating on water.

In Electron Cyclotron Resonance (ECR) electrodeless thrusters, which will be the focus of this paper, plasma is produced by electron heating via ECR effect and inelastic electron-neutral collisions. The electron temperatures reached via this heating mechanism are notably higher than those achievable with other electrodeless technologies like RF thrusters.[8] In a coaxial ECR thruster design configuration, the chamber is immersed in an axial magnetic field which diverges in the free space region downstream of the thruster body. The electrons gyrate around these field lines, generating a plasma-induced magnetic field which repels the applied field. The electrons are thus pushed downstream, whereas the heavier ions remain mostly unaffected. This creates an ambipolar electric field which, in turn, expands the ions radially and accelerates them axially. In essence the electron thermal energy, increased by the electric field component of the microwaves, is being converted into ion kinetic energy. The ambipolar plasma flows out of the chamber, expanding with the diverging magnetic field, until detachment from the field lines occurs. Thus, thrust is generated.

In short, ECR thrusters present the key advantage of being able to operate on multiple propellants using a design that is particularly well suited to low cost manufacturing, all the while boasting effective mitigation of the life limiting erosion issues seen in established EP technologies like GIEs and HETs. Water is particularly attractive as an alternative propellant, especially as theoretical analysis of water plasma in the context of electrodeless thrusters by Petro et al. concluded that water thruster efficiency would be extremely similar to argon if electron temperatures above 5 eV are reached.[9] The exciting potential of a water propelled ECR system, and its strong suitability to the rapidly growing small satellite market lead our consortium, a collaboration between AVS UK, the University of Surrey, STFC ISIS, and SSTL, to undertake the development of the world's first water propelled ECR thruster: AQUAJET.

With the support of a UK Space Agency NSTP Fast Track grant our consortium was able to design, build, and test an innovative, highly scalable test bed.[10] Three key experimental achievements of this project were successful operation of the breadboard thruster with xenon, argon, and water; stable firings at power levels up to 170 Watts, and demonstrated linear increase of performance (thrust and specific impulse) with power in the 20-200W range. Results and analysis from this experimental campaign are detailed in another paper from this session.[11]

Building on the success of the AQUAJET project, our consortium, expanded to include Viper RF, has undertaken a follow on NTSP Flagship project: AQUAJET|NJET|XJET. The goals of this project are multiple: design and build of three improved laboratory models capable of functioning on water, ammonia, and xenon propellants, custom design of a microwave generator spearheaded by Viper RF, and an advanced round of testing with scaling to higher power (approx. 400W). The following paper will detail the analytical modelling work conducted to evaluate the feasibility of ammonia operation, as well as the breadboard design upgrade work carried out thus far in the context of this Flagship project.

II. Rate Coefficient Analysis of H_2O and NH_3 Discharges

In the following section we compare the rate coefficients of inelastic electron impact processes in H_2O and NH_3 discharges in the context of electrodeless thruster operation. This rate coefficient analysis is followed by a critical assessment of the role of negative ion formation on plasma electronegativity and predicted positive ion fractions accelerated by the ambipolar sheath potential. The distribution of energy loss, ionization cost and thrust efficiencies of H_2O and NH_3 are then compared, allowing us to predict the performance of the two propellants prior to experimental testing.

A. Ionization Cross Sections and Rate Coefficients

The cross sections σ of electron impact ionization, molecular dissociation (fragmentation) via electronic excitation to repulsive states, and dissociative electron attachment (DEA) of H_2O and NH_3 molecules were taken from two review papers by Itikawa et al.[12,13] . Using the Maxwellian EVDF we can calculate the corresponding rate coefficients, see Fig. 1, with:

$$< \sigma v >= 4\pi \left(\frac{m_e}{2\pi k T_e}\right)^{3/2} \int v^3 \sigma(v) e^{-\frac{m_e v^2}{2kT_e}} dv. \tag{1}$$

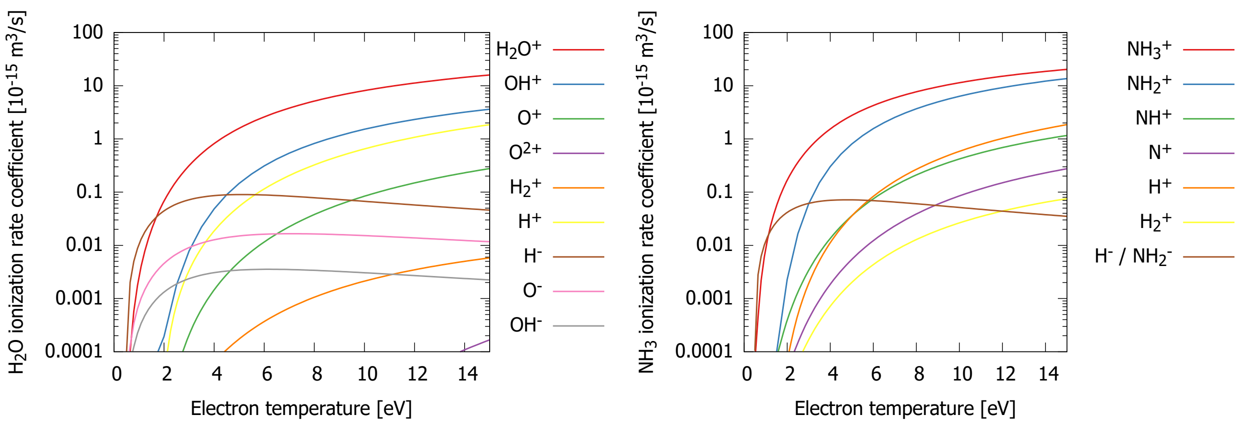

Figure 1: The electron impact ionization and dissociative electron attachment rate coefficients of H_2O molecules (left) and NH_3 molecules (right) by a Maxwellian electron population.

<u>NB:</u> The dissociative electron attachment rate coefficient of NH_3 in Fig. 1 corresponds to the total rate coefficient of negative ion formation with the yields of H^- and NH_2^- being almost equal[13] .

B. The Role of Ambipolar Plasma Potential and the Relevance of Negative Ion Formation

The thrust produced by an EP device is directly proportional to the specific impulse I_{SP}, which is in turn proportional to the velocity of the propellant and its mass. Assuming a collisionless sheath, the singly charged ions gain an energy (velocity) corresponding to the ambipolar plasma potential as they are repelled from the discharge.

Several expressions for the ambipolar sheath potential can be found in literature. In keeping with material published by Bibinov et al.[14] the sheath potential $|\Delta\Phi_{sh}|$ of a multi-species discharge can be expressed as seen in equation (2) where $\langle Q/M \rangle$ is the average charge to mass ratio of the ions with $Q = 1$ for the microwave discharge. For a single species discharge Petro et al.[9] use an alternate expression, shown below in eq. (3). We have chosen to use the latter for the rest of this section, and will bear in mind the assumptions carried with this choice.

$$|\Delta\Phi_{sh}| = \frac{T_e}{2}\left[5.67 - \ln\left\langle \frac{Q}{M} \right\rangle\right] \tag{2}$$

$$|\Delta\Phi_{sh}| = \frac{T_e}{2}\left[1 + \ln\left(\frac{m_i}{2\pi m_e}\right)\right] \tag{3}$$

Formula choice aside, it can be seen from both these equations that the plasma potential, and hence the thrust, is maximized when the electron temperature is high and the fraction of positive ions is as large as possible. Furthermore, as the plasma potential builds up to balance the mobilities of the negative and positive charges, the potential can be significantly reduced if the plasma is strongly electronegative. The electronegativity η being defined here as the ratio of negative to positive ion densities, i.e. $\eta = \frac{n_-}{n_+}$. It is therefore clear that the formation of negative ions could potentially affect the efficiency of an ambipolar thruster.

Following the same line of reasoning as Petro et al.[9] we determine that the ratio of negative ion and neutral densities is given directly by the ratio of the DEA and electron impact detachment rate coefficients, i.e

$$\frac{n_-}{n_n} = \frac{\langle \sigma_{DEA} v_e \rangle}{\langle \sigma_{det} v_e \rangle}. \tag{4}$$

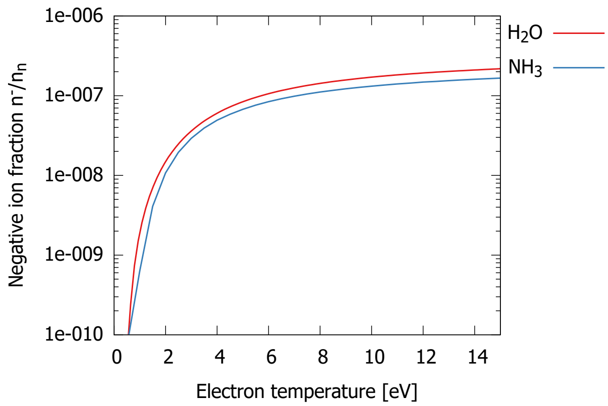

Figure 2: Steady-state ratio of negative ions to neutral particles as predicted by the particle balance model and corresponding rate coefficients.

Based on the ionization rate coefficients in Fig. 1 it is assumed hereafter that the dominating negative ion species in both discharges considered is H^-. Rate coefficients for electron impact dissociation of H^- are calculated using cross section data taken from Janev et al.[15] Thus, we are able to predict the negative ion to neutral density in H_2O and NH_3 discharges as a function of the electron temperature. This is shown on the left in Fig. 2.

It is found that in both discharges the negative ion fractions are well below 1 ppm of the neutral particle density. The result is reasonable as it implies that for a typical ionization degree of 1–10 %, the plasma electronegativity is on the order of 10^{-5}–10^{-4}. Therefore the role of negative ions on the thruster performance can be considered negligible in both discharges.

C. Positive Ion Fractions in the Plasma Sheath

The relative population densities of positive ions are derived from the ion density balance equation (eq. (5)) at steady-state, meaning $\frac{dn_+}{dt} = 0$, where the second term corresponds to the rate of ion losses by charge exchange and the third term corresponds to the ion losses characterized by confinement time τ.

$$\frac{dn_+}{dt} = n_e n_n \langle \sigma_{ion} v_e \rangle - n_+ n_n \langle \sigma_{cex} v_i \rangle - \frac{n_+}{\tau} = 0, \tag{5}$$

As in ionizing molecular plasmas the charge exchange rate can be considered negligible, we can express the ion density n_+ of each positive ion species as:

$$n_+ = n_e n_n \langle \sigma_{ion} v_e \rangle \tau. \tag{6}$$

In collisional discharges the ion confinement time is proportional to the characteristic plasma dimension L and the Bohm velocity v_B of the given ion species, i.e. $\tau = L/v_B$. Thus, it follows that the ion fractions for each species are a function of their relative ionization rates and Bohm velocities as

$$\frac{n_+}{n_{+,total}} = \frac{\langle \sigma_{ion} v_e \rangle / v_B}{\sum_j \left(\langle \sigma_{ion} v_e \rangle_j / v_{B,j} \right)} = \frac{\langle \sigma_{ion} v_e \rangle \sqrt{m_i}}{\sum_j \left(\langle \sigma_{ion} v_e \rangle_j \sqrt{m_{i,j}} \right)}, \tag{7}$$

where the last equality follows from $v_B = \sqrt{T_e/m_i}$ and the sum over j takes into account all positive ion species. The calculated positive ion fractions in H_2O and NH_3 discharges as a function of the electron temperature (for a Maxwellian EVDF) are shown in Fig. 3.

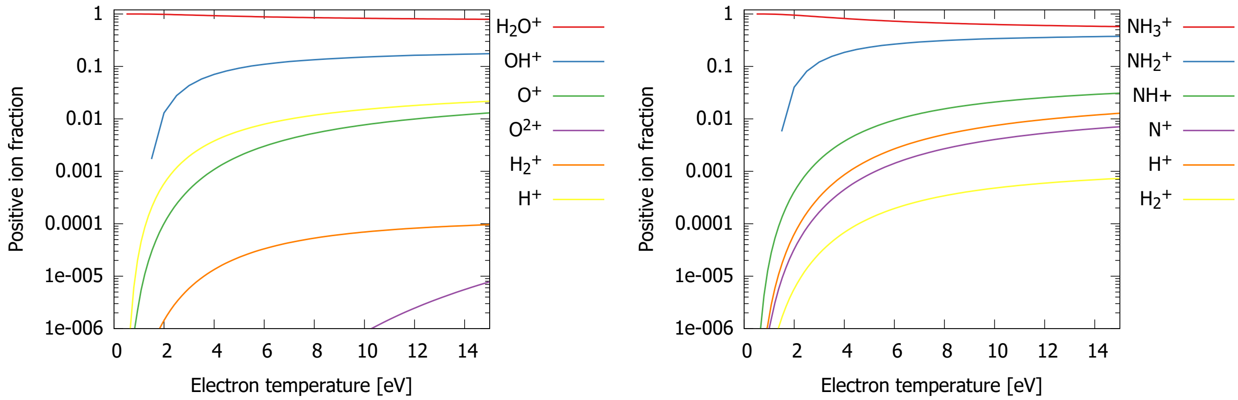

Figure 3: Distribution of positive ions in a H_2O (left) and NH_3 (right) plasma as a function of the electron temperature.

It can be seen from these plots that in the H_2O discharge the molecular H_2O^+ ions are found to account for more that 80 % of the positive ions in the temperature range relevant for the AQUAJET|NJET thrusters. In the NH_3 discharge the situation is more complex. Indeed, both NH_3^+ and NH_2^+ ions are found at relative fractions of several tens of percent at electron temperatures exceeding 5 eV. Nevertheless, as NH_3^+ is always the preferred ion formed in direct electron impact ionization and considering the mass difference between the two dominant species is only 1 a.m.u., the generated thrust can be approximated taking into account only the NH_3^+ ion mass.

The above analysis does not take into account non-ionizing dissociation of the molecules by electron impact or electron impact excitation to repulsive electronic (and ro-vibrational) states, which could affect the ion fractions. Figure 4 compares the rate coefficients of total ionization and dissociation to the ground state (X) of the OH-molecule in electron impact with H_2O based on cross sections reported by Itakawa et al.[12] Figure 5 compares the rate coefficients of total ionization and dissociative excitation by electron impact on the NH_3 molecule based on cross sections reported once again by Itikawa et al.[13]

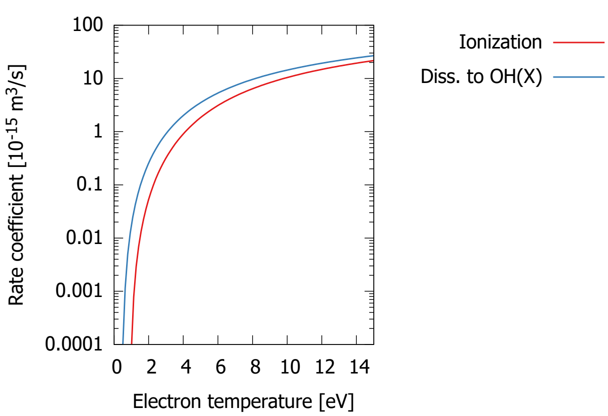

Figure 4: Rate coefficients of total ionization and non-radiative dissociation to OH(X)-state by electron impact on H_2O-molecules.

In the case of an H_2O discharge, although the dissociation cross section suffers from a reported uncertainty of approximately 30 %, it is evident that (non-radiative) electron impact dissociation probably affects the positive ion fraction in the discharge as the dissociation to ground state OH is favoured over ionization (predominantly to H_2O^+). Based on the rate coefficients plotted in Fig. 4 we know that if the ionization degree of the plasma is assumed to be between 1–10 % of the neutral H_2O density, the neutral OH fraction can be estimated to account for 2–20 % of the total neutral density. Thus, to validate our analysis it becomes imperative to compare the predicted ion fractions to measured ones. For this we plan to compare the ion fractions predicted by our analysis to the fractions we will measure in the project's upcoming experimental campaign, planned for spring of 2020.

In the case of the NH_3 discharge, assessing the effect of electron impact dissociation is more difficult. This is due to the lack of experimental cross sections. The only dissociation channel for which cross section data is found[13] is the electron impact excitation to repulsive A-states of the NH_3 molecule from where the decomposition into NH_2 and H occurs with a quantum yield of one independent of the ro-vibrational level.[16] Fig. 5 demonstrates that dissociation can be expected to affect the predicted positive ion fractions less in the case of NH_3 in comparison to H_2O. However, experimental evidence is still required to fully assess the uncertainty as there is no cross section data available for direct radiative or non-radiative dissociation of NH_3 by electron impact.

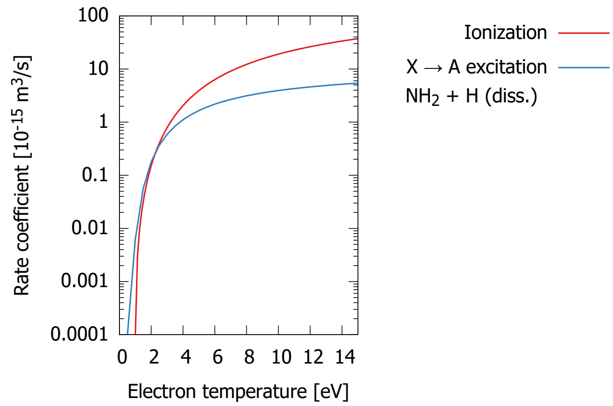

Figure 5: Rate coefficients of total ionization and dissociative excitation by electron impact on NH_3 molecules

D. Fractional Distribution of the Energy Loss

The fractional cost χ of the energy loss by process can be assessed by comparing the rate coefficient of a certain process to the total rate coefficient of all electron impact processes i.e.

$$\chi_i = \frac{\langle \sigma v \rangle_i E_i}{\Sigma_i \left(\langle \sigma v \rangle_i E_i \right)}, \tag{8}$$

where the energy E_i is the (average) energy dissipated in the collision by the conversion of the electron kinetic energy.

The fractional distribution of the energy loss in an H_2O discharge has been estimated by Petro et al.[9] This analysis can be simplified by excluding reactions like direct rotational excitation, vibrational excitation, and elastic scattering of electrons. Indeed, thruster performance is expected to be low in the electron temperature range at which these reactions are dominant (less than 3 eV), and it would be impractical to assess the fractional distribution of electron losses in a regime that needs to be avoided in the first place. The reactions that need to be considered to calculate the distribution of energy loss include ionization, electronic excitation, and direct dissociation.

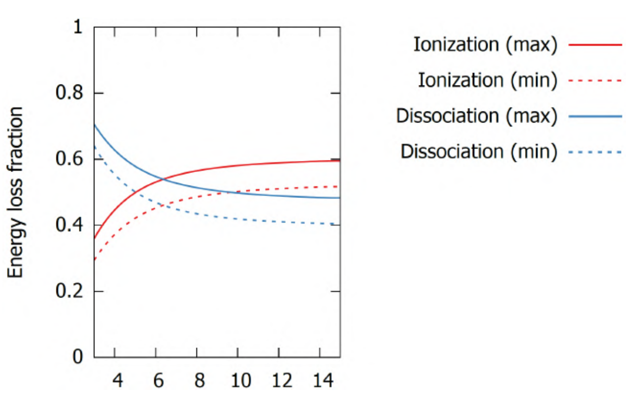

Figure 6: Fractional distribution of energy loss in H_2O discharge. Ionization and dissociation refer to reactions $H_2O + e \rightarrow H_2O^+ + 2e$ and $H_2O + e \rightarrow OH(X) + H$. The maxima and minima are shown to highlight the uncertainty related to the vibrational distribution of the molecules.

Based on the positive ion fractions plotted in Fig. 3, we only take into account the ionization reaction $H_2O + e \rightarrow H_2O^+ + 2e$ that has a reaction enthalphy of 12.621($\pm$0.002) eV.[17] This can be considered accurate if the ionization degree is below 10 %. The energy loss by electronic excitation cannot be taken into account due to insufficient cross section data. As for direct dissociation, data exists for reactions $H_2O + e \rightarrow OH(X) + H$ and $H_2O + e \rightarrow O(^1S) + H_2$. As the cross section of the latter reaction is more than two orders of magnitude smaller and has a higher threshold than the first reaction, it is omitted. The minimum energy of the dissociation to OH(X) (and H) is 5.0992($\pm$0.003) eV[18] but the observed threshold is approximately 7.0 eV.[19] This discrepancy is probably due to the ro-vibrational distribution of the molecules. Both values are used for estimating the contribution of dissociation on the distribution of electron energy loss shown in Fig. 6.

Fig. 6 confirms that in an H_2O discharge it can always be expected that a significant fraction of the power will be dissipated by molecular fragmentation. This is especially the case at low electron temperatures (< 6 eV), where the majority of the energy is dissipated to molecular dissociation. Wasting power to dissociation results in lower thrust compared to noble gas propellant, as was observed experimentally for AQUAJET breadboard thruster operation at electron temperatures of less than 5 eV.[11] We expect that achieving electron temperatures exceeding 10 eV will lead to a much more favourable distribution of energy loss between ionization and molecular dissociation, allowing for improved thruster efficiency, as was achieved for the ONERA ECR thruster.[20]

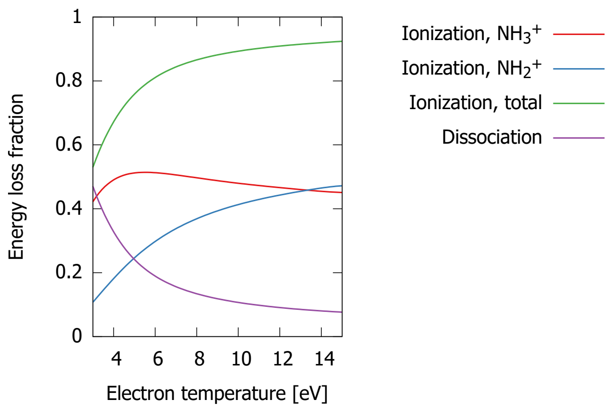

Figure 7: Fractional distribution of energy loss in NH_3 discharge. Ionization and dissociation refer to reactions $NH_3 + e \rightarrow NH_3^+ + 2e$, $NH_3 + e \rightarrow NH_2^+ + H + 2e$ and $NH_3(X) + e \rightarrow NH_3(A) + e \rightarrow NH_2 + H$, respectively.

In the case of NH_3 the only reactions for which sufficient cross section data exist are ionization and electronic excitation to the repulsive A-state. The state A is the lowest singlet state and the transition from the ground state to the vibrational levels of the A-state is dipole allowed. From these facts it can be concluded that the cross sections for the excitation of other states can be expected to be not much larger if not smaller than that for the X$\rightarrow$A transition. In the case of NH_3 both ionization reactions $NH_3 + e \rightarrow NH_3^+ + 2e$ and $NH_3 + e \rightarrow NH_2^+ + H + 2e$ must be taken into account. The recommended value for the ionization potential of NH_3 is 10.070($\pm$0.02) eV[17] whereas the reaction enthalpy of the latter electron impact ionization reaction is 15.73($\pm$0.02) eV.[21] The energy of the dissociation via electronic excitation to the repulsive A-states used in the original work by Harshbarger et al. determined that the excitation cross section is 6.390 eV.[22] This does not take into account excitations to different vibrational levels. Taking into account the lack of cross section data and all related uncertainties this can be considered to be only a minor problem. The resulting uncertainty is most likely similar to that plotted for H_2O. The distribution of energy loss in NH_3 discharge is shown hereabove in Fig. 7.

Using the fractional costs calculated, we can finally plot the ionization cost ψ_{ion} for the H_2O and NH_3 discharges, see Fig. 8, using the following formula:

$$\psi_{ion} = \frac{\Sigma \chi_j E_j}{\chi_{ion,total}}. \tag{9}$$

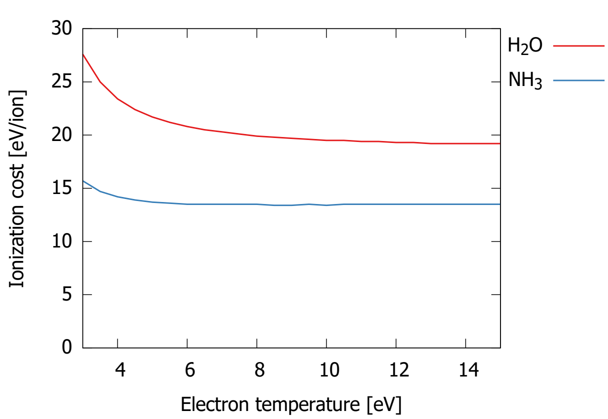

Figure 8: The estimated ionization cost (eV/ion) in H_2O and NH_3 plasmas.

Bearing in mind that the 10–15% fraction of OH^+ would increase the ionization cost, i.e. that the given value in the H_20 case must be regarded as the lower limit, we can conclude from Fig. 8 that NH_3 discharge can be expected to be better in terms of power efficiency. However, the lack of cross section data results in significant uncertainty.

Assuming that the radial losses (transverse to the magnetic field of 600–800 mT) are negligible[23] and ignoring the magnetic mirror confinement of the highly collisional plasma equating the losses towards the back wall and exhaust allows expressing the thrust efficiency η_T as[9]

$$\eta_T = \frac{P_{beam}}{P_{in}} = \frac{\eta_{MW}\eta_D|\Delta\Phi_{sh}(T_e)|}{4T_e + 2|\Delta\Phi_{sh}(T_e)| + 2\psi_{ion}(T_e)}, \tag{10}$$

where η_{MW} and η_D are the microwave coupling and beam divergence efficiency, and $|\Delta\Phi_{sh}|$ is given by eq (3). Thus, the ionization-to-thrust efficiency $\eta_{T,ion}$ is simply

$$\eta_{T,ion} = \frac{\eta_T}{\eta_{MW}\eta_D} = \frac{|\Delta\Phi_{sh}(T_e)|}{4T_e + 2|\Delta\Phi_{sh}(T_e)| + 2\psi_{ion}(T_e)}. \tag{11}$$

This is shown in Fig.9 as a function of the electron temperature for H_2O and NH_3 plasmas. In the case of H_2O only H_2O^+ ions are taken into account whereas for NH_3 the predicted fractions of NH_3^+ and NH_2^+ are used to determine the sheath potential as a function of the electron temperature. Figure 9 also shows the ratio of the ionization-to-thrust efficiencies of NH_3 and H_2O discharges. As the same assumptions are made for the ambipolar thrust generated by the two discharges, the given ratio can be used as an indicative measure of the expected performance difference between the two propellants despite the thrust efficiencies carrying relatively large uncertainties. It turns out, that the thrust efficiency is dominated by the effect of the electron temperature on the sheath potential, while the actual ionization cost differences ultimately correspond to a relatively small efficiency improvement of NH_3 over H_2O.

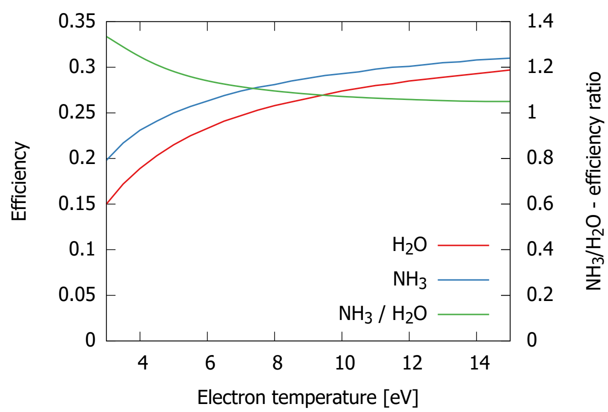

Figure 9: The estimated ionization-to-thrust efficiency of H_2O and NH_3 plasmas of the ambipolar thruster. The ratio of the efficiencies of NH_3 and H_2O is given on the secondary axis.

III. Design Upgrades for the AQUAJET Thruster

Based on the rate coefficient analyses of H_2O and NH_3 discharges detailed in the previous section we were successful in confirming the viability of thruster operation with ammonia. While we can expect, and have confirmed in the case of H_2O plasma,[11] lower performance for these molecular propellants compared to more commonly used noble gases, we believe their system-level benefits will outweigh the performance penalty incurred. This section will describe the design upgrades that have been made to the breadboard thruster. Upgrades which we are confident will further improve performance.

A. Brief Description of the AQUAJET Breadboard

With the support of NSTP Fast Track grant number NSTP3-FT-63, our consortium was able to design and build a highly modular breadboard thruster. The design of this breadboard is described in both proceedings from the 2018 Space Propulsion Conference,[10] and in a sister paper from this session by Moloney et al.[11]

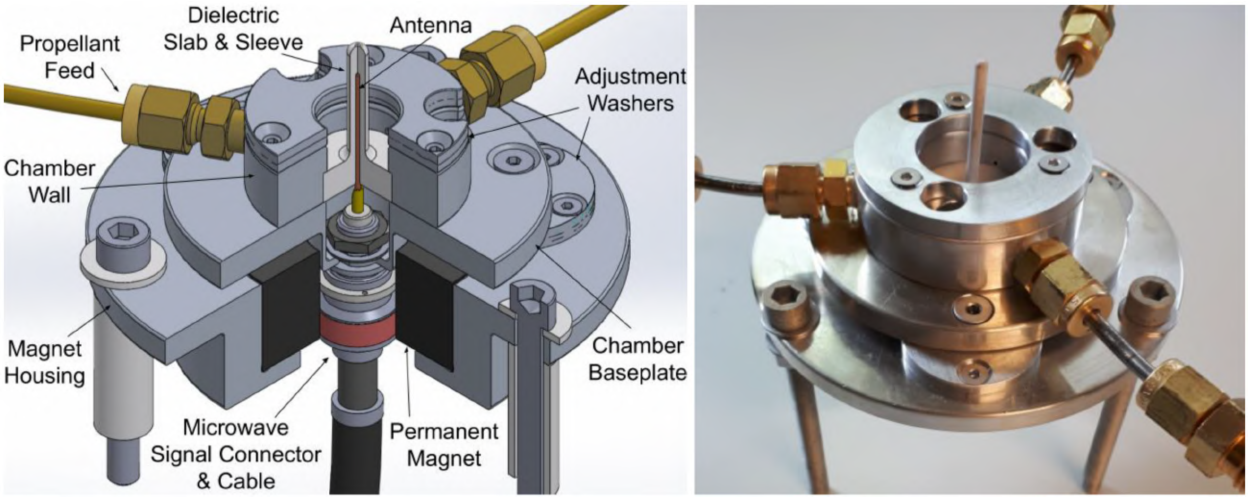

Figure 10: On the left: Partial cross-section schematic of the AQUAJET thruster. On the right: Photograph of the AQUAJET thruster assembly.[11]

Fig.10 shows key components of the ECR breadboard thruster. The E field is produced by a wire type copper antenna fed by a 2.45 GHz microwave coaxial line. To protect it from erosion, the antenna is covered by a dielectric sleeve made of a moisture resistant BN grade. The magnetic nozzle is produced by an annular SmCo magnet sitting upstream of the chamber. Propellant is injected into the chamber radially by three equally spaced brass Swagelok fittings. Finally, a set of interchangeable magnet and chamber length washers allowed us to test different ECR zone positions and chamber lengths. Additionally, three different chamber wall pieces, of 8, 10 and 12 mm radius, were machined.

B. Microwave Line Improvements and Impedance Matching Considerations

As is explained by Moloney et al.,[11] while the measured thrust efficiencies for the AQUAJET breadboard ranged only between 0.1 and 2.5%, it is possible, if we take into account the estimated power losses in the microwave line, that the efficiencies may have in reality ranged between 0.1-8.2%. Indeed, the thruster was tested at power levels from 17-171W. However, if we take into account estimated line losses and uncertainties, in actuality, the absorbed power may have been between 10-120W.

To address this issue we will be integrating network diagnostics into the next experimental campaign's text matrix. Additionally, the microwave line has been modified, as can be seen in Fig. 11. This is thanks to our newly designed torsional thrust balance and to the custom designed microwave power supply unit currently being built by Viper RF. The fact that Viper's PSU operates in vacuum removed the need for any vacuum feedthrough. Furthermore, AVS' new torsional thrust balance, as described by Swar et al.,[24] employs wireless microwave power transmission and precludes the need for a DC block. In the cases where we would be testing without the torsional thrust balance (for ammonia testing for example), we would attach the DC block directly to the Viper RF generator.

Antenna impedance matching was an important consideration for the design upgrade. Efforts had been made in the breadboard's design phase to minimise impedance mismatch, namely with the help of an electromagnetic frequency-domain model of the chamber-antenna system using Multiphysics software.[10] This modelling effort was confirmed experimentally as the chamber configurations for which the impedance matching was the most optimal showed the lowest values of reflected power.[11] Despite this, measured reflected

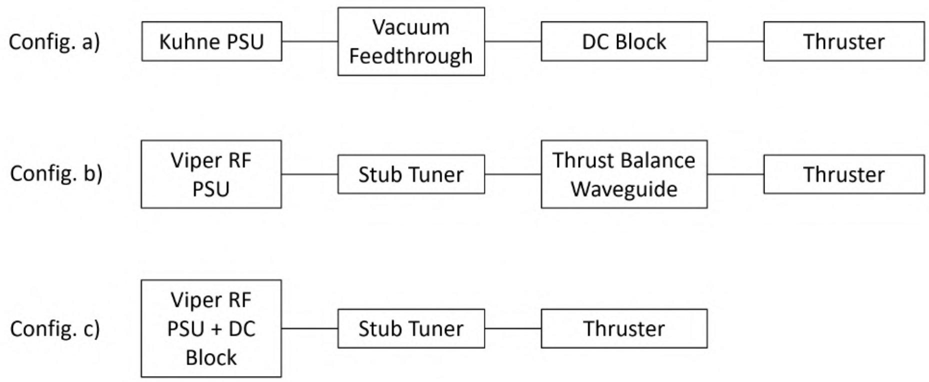

Figure 11: Configuration a: MW line schematics in the AQUAJET breadboard. Configurations b and c: Two possible MW block diagrams for the upgraded breadboard model.

power remained unacceptably high. In an effort to address this issue, provisions have been made to integrate a stub tuner into the microwave line of the improved breadboard, see Fig 11.

In addition to this, Viper RF is integrating an automatic real-time frequency feedback loop into the microwave PSU. This feedback loop, which can be disabled to allow for fixed frequency generation, modifies the frequency in the 2.3-2.54 GHz range in such a way as to minimize the detected output reflected power. It is currently being implemented as an external microcontroller demonstrator, thus enabling sufficient flexibility to be able to programme the software externally and independently from the microwave generator unit.

C. Key Component Upgrades

Another salient feature of the design upgrade was the improvement of two key components: the final TNC connector in the microwave coaxial line and the chamber base plate.

In the AQUAJET breadboard, see Fig. 10, the final coaxial cable connected to a TNC type female connector with a solder cup termination and PTFE insulation. The copper antenna was then simply soldered to the connector using vacuum compatible solder. During thruster operation, this component experienced a highly localized temperature peak at the solder connection point, we suspect due in large part to the impedance mismatch. This resulted in significant PTFE and solder melting issues. Fig. 12 shows one of these damaged connectors.

Figure 12: Pictures of the TNC connector damage sustained during the breadboard testing campaign.

To ensure that local heating of the antenna would no longer be an issue, a custom TNC type connection was designed. This connector features Macor insulators, a titanium shell, and a titanium central conducting pin. Macor was chosen for its high continuous operating temperature, 800°C, and the fact that its coefficient of thermal expansion matches that of titanium quite closely. The central conducting pin of this connector ends in a screw termination, to strengthen the connection point and to avoid any possible melting.

The thruster chamber base plate was also modified. Fig. 13 shows simulation results for the E field strength in a cut plane of the breadboard thruster operating at 2.45 GHz and 90W input power. These results were obtained in Altair's RF modelling software, FEKO, using a highly detailed model of the breadboard geometry constructed. It can be seen from Fig. 13 that there is an increase in E field strength in the empty region between the chamber base plate and the back of the chamber dielectric, where the antenna soldered connection point sits. Faced with concerns that some of the power lost may have been dissipated to the creation of a PTFE and silver solder plasma in this region, upstream of the chamber, lead to the design of an improved baseplate leaving minimal space around the TNC to antenna screw connection upstream of dielectric antenna sleeve and backplate.

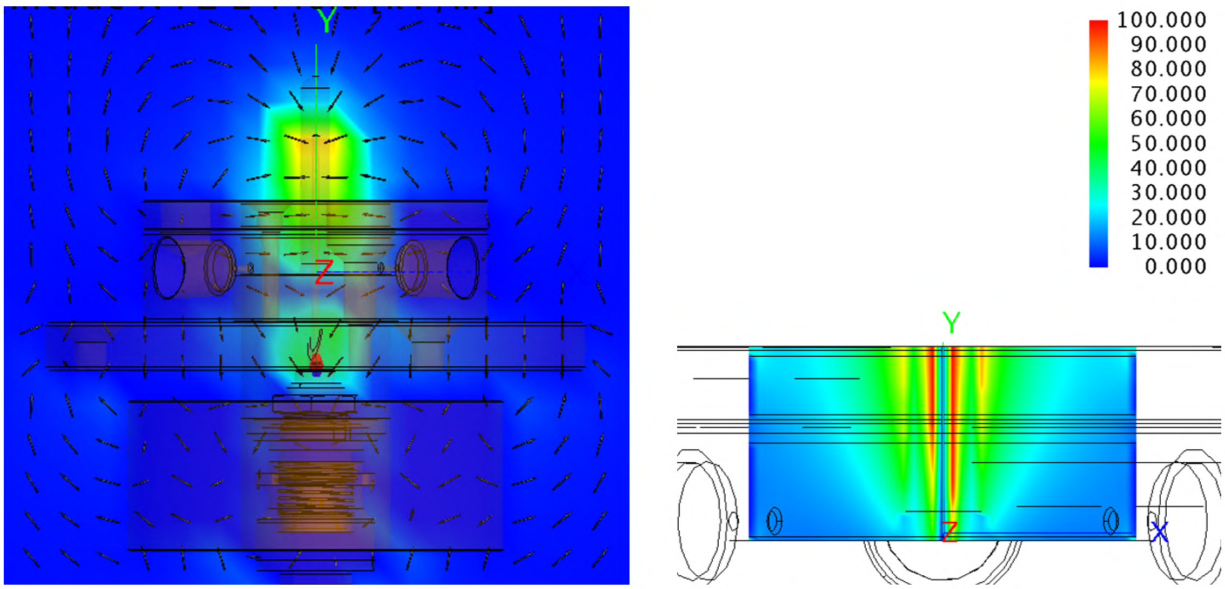

Figure 13: Instantaneous E-field magnitude (kV/m) in the AQUAJET breadboard, full thruster cut plane view (left) and chamber volume cut plane view (right)

In short, design upgrades for the AQUAJET breadboard focused on improvements to the microwave line, the design of a bespoke coaxial connector, and some small redesign of supporting geometry parts.

IV. Conclusion

Analytical plasma modelling was undertaken to evaluate the feasibility of thruster operation with ammonia based on H_2O plasma discharge modelling work by Petro et al.[9] Assuming, in both H_2O and NH_3 discharges, that H^- is the dominant negative ion species we find that the negative ion fractions in these discharges are well below 1ppm of the neutral particle density, meaning the role of negative ion formation on thruster performance can be considered negligible. Analysis of the positive ion fractions in an H_2O discharge revealed H_2O^+ is largely dominant, while in an NH_3 discharge both NH_3^+ and NH_2^+ are found in significant fractions at temperatures above 5 eV. The impact of non-ionizing dissociation and excitation to repulsive electronic states on these analyses calls for validation of the results by comparison with experimental data. This data will be collected in the project's upcoming experimental test campaign, planned for spring of 2020. As in the case of water discharge, specifically at electron temperatures of less than 6 eV, a significant amount of power is lost to molecular fragmentation, the ionization cost of ammonia appears much more favorable. This difference is ultimately only minimally reflected in terms of thrust efficiency as we found that at the electron temperatures of interest the ionization to thrust efficiency of water and ammonia discharges are comparable. Analytical ammonia plasma modelling work was accompanied by a design upgrade of the AQUAJET breadboard thruster based on experimental campaign results presented in this session by Moloney et al.[11] The upgrade work centered on improvements to the microwave coaxial line and modification of several central components. The integration of a bespoke vacuum compatible microwave PSU, with a real-time frequency feedback loop optimizing for minimal reflected power, helped significantly simplify the breadboards coaxial line. Additionally, incremental improvements to the breadboard supporting parts will further reduce power loss. Future work from the consortium will include the build of the AQUAJET|NJET|XJET laboratory models at AVS UK Ltd., followed by an extensive test campaign at the Surrey Space Center.

Acknowledgments

The AQUAJET|NJET|XJET project is funded by the UK Space Agency's National Space Technology Programme (grant reference number NSTP3 FS021). The authors are very grateful for the UK Space Agency's continued support.

References

[1]Fischer, J., Ferriauolo, B., Hertel, T., Monheiser, J., Barlog, C., Allen, M., Myers, R., Hoskins, A., Bontempo, J., Nazario, M., Shastry, R., Soulas, G., and Aulisio, M., "NEXT-C Flight Ion Propulsion System Development Status," *The 35th International Electric Propulsion Conference*, Atlanta, 2017.

[2]Koppel, C., Marchandise, F., Estublier, D., and Jolivet, L., "The SMART-1 Electric Propulsion Subsystem in Flight Experience," *40th AIAA/ASME/SAE/ASEE Joint Propulsion Conference and Exhibit*, Fort Lauderdale, 2004, pp. 34-35.

[3]Starlink Press Kit, URL: *https://www.spacex.com/sites/spacex/files/starlinkpresskit.pdf* [cited 11 September 2019].

[4]Rafalskyi, D., and Aanesland, A., "Brief Review on Plasma Propulsion with Neutralizer-free Systems," *Plasma Sources Science and Technology*, Vol. 25, No. 4, 2016.

[5]Charles, C., Boswell, R. W., Laine, R., and MacLellan, P., "An Experimental Investigation of Alternative Propellants for the Helicon Double Layer Thruster," *Journal of Physics D: Applied Physics*, Vol. 41, No. 17, 2008.

[6]James, K., Bodnar, M., Freedman, M., Osborne, L., Grist, R., and Hoyt, R., "HYDROS: High Performance Water-Electrolysis Propulsion for Cubesats and Microsats," *Advances in the Astronautical Sciences Guidance, Navigation and Control*, Vol. 159, 2017.

[7]Bonin, G., Foulds, C., Armitage, S., and Faber, D., "Prospector-1: the First Commercial Small Spacecraft Mission to an Asteroid," *30th Annual AIAA/USU Conference on Small Satellites*, Logan, 2016.

[8]Packan, D., Elias, P. Q., Jarrige, J., Merino Martinez, M., Sanchez Villar, A., Ahedo Galilea, E. A., Peyresoubes, G., Holste, K., Klar, P., Bekemans, M., Scalais, T., Bourguignon, E., Zurbach, S., Mares, M., Hoque, A., Favier, P., "The MINOTOR H2020 Project for ECR Thruster Development," *The 35th International Electric Propulsion Conference*, Atlanta, 2017.

[9]Petro, E. M., Sedwick, R. J., "Effects of Water-Vapor Propellant on Electrodeless Thruster Performance," *Journal of Propulsion and Power*, Vol. 33, No. 6, 2017, pp. 1410-1417.

[10]Staab, D., Frey, A., Garbayo, A., Shadbolt, L., Lucca Fabris, A., Gurciullo, A., Grondein, P. E., Moloney, R., Faircloth, D., and Lawrie, S., "AQUAJET: an Electrodeless ECR Water Thruster," *Space Propulsion Conference Proceedings*, Seville, 2018.

[11]Moloney, R., Karadag, B., Lucca Fabris, A., Staab, D., Frey, A., Garbayo, A., Shadbolt, L., Rosati Azevedo, E., Faircloth, D., Lawrie, S., and Tarvainen, O., "Experimental Validation and Performance Measurements of an ECR Thruster Operating on Multiple Propellants," *The 36th International Electric Propulsion Conference*, Vienna, 2019.

[12]Itikawa, Y., and Mason, N., "Cross Sections for Electron Collisions with Water Molecules," *Journal of Physical and Chemical Reference Data*, Vol. 34, No. 1, 2005, pp. 1-22.

[13]Itikawa, Y., "Cross Sections for Electron Collisions with Ammonia," *Journal of Physical and Chemical Reference Data*, Vol. 46, No. 4, 2017.

[14]Bibinov, N. K., Bratsev, V. F., Kokh, D. B., Ochkur, V. I., and Wiesemann, K., "Spectroscopic Determination of the Cold Electron Population in Very Low Pressure ECR Discharges in N_2/He Mixtures," *Plasma Sources Science and Technology*, Vol. 14, No. 1, 2005, pp. 109.

[15]Janev, R. K., Reiter, D., and Samm, U., *Collision Processes in Low-temperature Hydrogen Plasmas*, Forschungszentrum Jülich, Zentralbibliothek, 2003.

[16]Back, R. A., Koda, S., "The Photodissociation of Ammonia in the A←X Absorption System. Part II. Translational Excitation of the Hydrogen Atoms Produced and the Mechanisms of the Predissociation," *Canadian Journal of Chemistry*, Vol. 55, No. 8, 1977, pp. 1387-1395.

[17]Lias, S. G., "Ionization Energy Evaluation," *NIST Chemistry WebBook, NIST Standard Reference Database Number 69*, 2005.

[18]Ruscic, B., Wagner, A. F., Harding, L. B., Asher, R. L., Feller, D., Dixon, D. A., Peterson, K. A., Song, Y., Qian, X., Ng, C. Y., and Liu, J., "On the Enthalpy of Formation of Hydroxyl Radical and Gas-phase Bond Dissociation Energies of Water and Hydroxyl," *Journal of Physical Chemistry A*, Vol. 106, No. 11, 2002, pp. 2727-2747.

[19]Harb, T., Kedzierski, W., and McConkey, J.W., "Production of Ground State OH Following Electron Impact on H_2O," *The Journal of Chemical Physics*, Vol. 115, No. 12, 2001, pp. 5507-5512.

[20]Cannat, F., Lafleur, T., Jarrige, J., Chabert, P., Elias, P. Q., and Packan, D., "Optimization of a Coaxial Electron Cyclotron Resonance Plasma Thruster with an Analytical Model," *Physics of Plasmas*, Vol. 22, No. 5, 2015, pp. 053503.

[21]Dibeler, V. H., Walker, J. A., and Rosenstock, H. M., "Mass Spectrometric Study of Photoionization V. Water and Ammonia," *Journal of Research of the National Bureau of Standards*, Vol. 70A, No. 6, 1966, pp. 13-05.

[22]Harshbarger, W. R., Skerbele, A., and Lassettre, E. N., "Generalized Oscillator Strength of the A←X Transition of Ammonia," *The Journal of Chemical Physics*, Vol. 54, No. 9, 1971, pp. 3784-3789.

[23]Ahedo, E., and Navarro-Cavalle, J., "Helicon Thruster Plasma Modeling: Two-dimensional Fluid-Dynamics and Propulsive Performances," *Physics of Plasmas*, Vol. 20, No. 4, 2013, pp. 043512.

[24]Swar, K., Staab, D., Garbayo, A., Shadbolt, L., Masillo, S., Lucca Fabris, A., Karadag, B., Moloney, R., "Design and Testing of a μN-mN Torsional Thrust Balance with Wireless Microwave Power Transmission," *The 36th International Electric Propulsion Conference*, Vienna, 2019.